Increasing the Test-Volume of Open TEM Cells by Using an Asymmetric Design

C. Spindelberger[*], G. Giannetti[†], and H. Arthaber[*]
[*] Technische Universität Wien, Vienna, Austria
[†] University of Florence, Florence, Italy
christian.spindelberger@tuwien.ac.at

***Abstract*—Open transverse electromagnetic (TEM) cells offer a low-cost solution for radiated pre-compliance measurements. Usually, available cells are implemented as a symmetric stripline. The main drawback of this technique is the equal distance between the inner and outer conductors, limiting the vertical space for the equipment under test. Throughout this paper, the potential of an asymmetric stripline approach is analyzed to provide test-volume space more efficiently. The main goal was to design a low-cost structure which is easy to build and gives the opportunity to make radiated pre-compliance measurements up to 1 GHz with a budget below 500 €. The initial geometry of the cell was derived analytically, optimized by 3D-EM simulations, and manufactured in-house. For verification purposes, S-parameter and field-probe measurements have been made and compared to simulation results. It is shown that the field homogeneity complies to *IEC 61000-4-20* for the desired bandwidth having a cubic test-volume with an edge-length of 100 mm.**

***Index Terms*—Electromagnetic interference (EMI), Electromagnetic compatibility (EMC)**

I. Introduction

Available transverse electromagetic (TEM) cell structures for pre-compliance purposes are usually symmetric and open. This paper addresses *CISPR* bands C and D covering a frequency range from 30 MHz–1 GHz. According to [1], the size of the equipment under test (EUT) is limited to a third of the septum height for such wavelengths. In [2], [3], and [4] different designs for the target frequency bands are presented. The maximum achieved septum height is 90 mm which corresponds to a cubic uniform test-volume (UTV) with an edge-length of 30 mm only. Furthermore, the characterization of the electric field has not been considered in any of the mentioned papers.

To increase the EUT size, an asymmetric TEM cell, depicted in Figure 1, is investigated with a target septum height of 300 mm. The main design criteria of the cell are based on S-parameters and the field homogeneity in the UTV specified by *IEC 61000-4-20* [5]. Present higher order modes need to be considered as they introduce unintentional field components. The desired TEM mode is mostly influenced by the bending edges of the tapering. One approach to enhance the suppression of higher order modes is to lower the vertical angle. The drawback of this method is an enlarged cell, prone to modal dispersion effects. Additionally, the cross-section of the tapering changes over distance and impedes the matching of the cell. Throughout this paper, the most relevant design

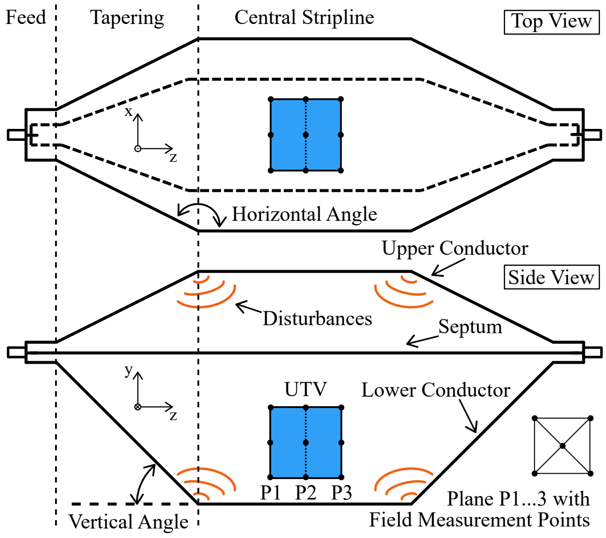

Fig. 1. Sketch of an asymmetric TEM cell with the respective coordinate system.

trade-offs regarding field requirements and return loss (RL) are discussed.

Another important aspect for pre-compliance equipment are the costs. Fully compliant cells for the desired frequency range and EUT size, are usually GTEM cells. The closed structure, a distributed termination, and the use of absorbers makes them relatively expensive and difficult to manufacture in-house using standard tools. As TEM cells do not require absorptive material and the termination can be realized with a connectorized load, they represent a low-cost alternative. Thus, the design of an open TEM cell which is easy to build having a budget of a few hundred Euros is pursued.

The content is organized as follows. In Section II, an initial geometrical approach of the cell is derived analytically. With 3D-EM simulations, the structure is analyzed and design trade-offs are examined. The realized structure is characterized in terms of S-parameters and field homogeneity in Section III. Lastly, a conclusion of the achieved performance is provided in Section IV.

II. Design of the TEM Cell

Referring to Figure 1, the TEM cell is composed of three sections. The symmetric stripline feed connects via a tapered section to the asymmetric central stripline where the EUT is placed. The most important performance metrics for the design are the insertion loss (IL), RL, and the field homogeneity. Besides the losses of the material, the IL gives an indication of the amount of radiated power. The matching influences the absolute measurement accuracy [6]. As EMI receivers are specified having an RL larger than $10\,\mathrm{dB}$, this value is set as design goal [7]. The field components in the UTV are measured with a field probe at specified planes in P1–3 (see Figure 1). The respective procedure is explained in [8]. The *IEC 61000-4-20* standard is satisfied if the following two requirements are fulfilled for 4 out of 5 points at each plane over frequency:

- The variation of the magnitude $|\vec{E}|$ is not larger than $6\,\mathrm{dB}$ for the chosen points.
- The longitudinal ($|E_z|$) and horizontally ($|E_x|$) polarized field components are at least $6\,\mathrm{dB}$ smaller than the magnitude $|\vec{E}|$.

In the following, the theoretical approaches to achieve a septum height of $300\,\mathrm{mm}$ and a bandwidth of $1\,\mathrm{GHz}$ are investigated. The target impedance is $50\,\Omega$ and the UTV is located in the middle of the cell with a height offset of $21\,\mathrm{mm}$. Due to the desired simple fabrication process, only linear geometries have been considered.

A. Feed

As starting point, the feed (see Figure 2) was designed separately. To reduce mechanical stress onto the inner lead of the coaxial connector, the transition to the symmetric stripline was implemented with a $1.5\,\mathrm{mm}$ *FR4* printed-circuit board (PCB). The PCB is clamped by two aluminium bars. The cross-section of the stripline was modeled analytically for a planar structure using air as dielectric [9]. With 3D-EM simulations, influences of the PCB material were investigated. The transition caused mismatch between the stripline and the connector was reduced by introducing an air-gap of $2\,\mathrm{mm}$ between them.

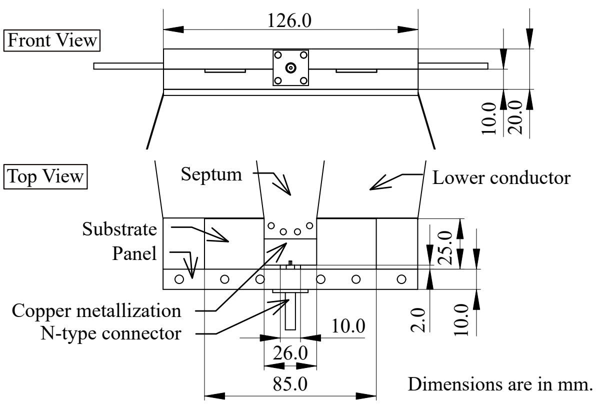

Fig. 2. Drawings of the realized feed.

B. Central Stripline

The cross-section of the central stripline is depicted in Figure 3. The target UTV has an edge-length l_{UTV} of $100\,\mathrm{mm}$. According to [1], l_{UTV} is limited by: $\min\{0.6w_s, 0.6l_s, h_s/3, \lambda(f = f_{max})\}$. Due to the tapering, the length of the cell strongly depends on the vertical size. Hence, $h_s/3$ is assumed to be the smallest factor for a maximum frequency of $1\,\mathrm{GHz}$. The septum height results in $h_s = 3\,l_{\mathrm{UTV}} = 300\,\mathrm{mm}$. To achieve an impedance of $50\,\Omega$, the distance between the upper conductor and the septum was calculated by the method from [10]. The remaining parameters of the central stripline have been adopted from [4]: $w_c = 300\,\mathrm{mm}$, $l_c = l_s = 465\,\mathrm{mm}$, $\alpha = 30°$. For first performance evaluations, the ratio w_s/w_c was investigated. The best results in terms of RL and field homogeneity were found for a ratio of 0.65. Next, the optimum length l_c was examined. In principal, higher order modes decay exponentially in the central stripline part [11]. For a limited range of $200\,\mathrm{mm} \leq l_c \leq 600\,\mathrm{mm}$, the simulation results indicated that a trade-off between the RL and field homogeneity had to be found. The cell showed the best performance having a length of $500\,\mathrm{mm}$. Due to modal dispersion, the RL could not be kept in the desired range for larger values. To further improve the matching, l_s was slightly reduced to $465\,\mathrm{mm}$.

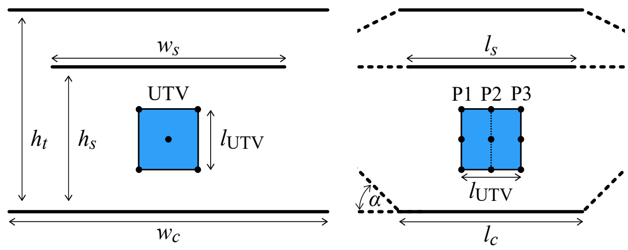

Fig. 3. Central stripline: cross-section (left) and side-view (right).

C. Tapering

The field homogeneity suffers from changes of the cross-sections dimensions. As the bending edges of the tapering are the most critical transition of the TEM cell, the focus was put on the vertical angle for the design. A low angle reduces field perturbations at the central stripline input. In contrast, the tapering length increases, causing long edges which are prone to manufacturing deviations using a handsaw. For an angle of $25°$, the best compromise between matching and field homogeneity was achieved at a total TEM cell length of $1.8\,\mathrm{m}$.

D. Material and Budget

The material costs of the realized cell, depicted in Figure 4, are composed as follows. The Aluminium sheets are $3\,\mathrm{mm}$ thick with a price of approx. 150 €. The Teflon pillars have a diameter of $35\,\mathrm{mm}$ and were about 200 €. For the rest of the parts, comprising the PCB material, the connectors, and the screws a budget of 150 € has to be expected. In total, the material for the cell costs 500 €.

III. Characterization of the TEM Cell

In the following, the derived S-parameters and field requirements of the simulation are compared to the realized prototype.

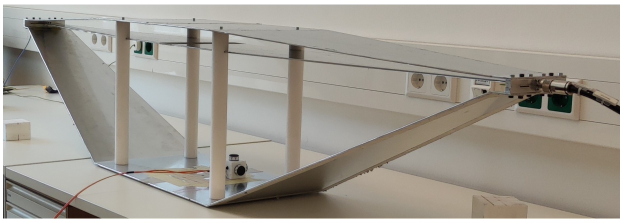

Fig. 4. Realized TEM cell while performing field measurements.

The simulations were performed with *HFSS* using standard materials and open radiation boundaries [12]. The used connector *Amphenol 172224* was modeled by its cross-section with a Teflon dielectric. For all simulation results, waveguide ports have been utilized. The electric field components were derived by an analytical calculator provided by the simulator.

A. S-parameters

The simulated and measured S-parameters are given in Figure 5. The targeted matching of $-10\,\mathrm{dB}$ is met over the whole frequency range. One can see, that the $|S_{11}|$ is slightly shifted in frequency and the measured $|S_{21}|$ is higher. In the simulation, an open boundary surrounding the cell was assumed. In laboratory conditions this test site cannot be realized. Consequently, the measured characteristics slightly changed. Furthermore, the metal sheets sag down due to mechanical stress causing an overall length mismatch which further influences the frequency shift. The results below $100\,\mathrm{MHz}$ show an $|S_{11}|$ in the range of $-40\,\mathrm{dB}$. To simulate such small reflections, a substantial increase in simulation time has to be expected to get results with the required accuracy. Furthermore, standard connectors are usually specified with a much higher worst case matching, i.e., $|S_{11}| < -17.7\,\mathrm{dB}$. As the TEM cell shows an excellent performance in this frequency range, deviations between simulation and measurement results have not been further investigated.

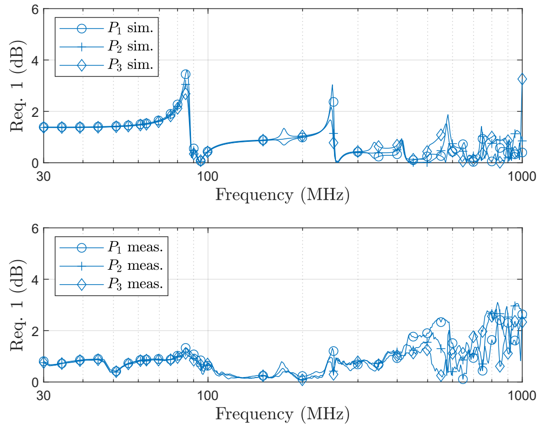

Fig. 6. Measured and simulated first field requirement.

B. Field Uniformity

In Figure 6, the results of the first field requirement, explained in Section II, are visualized. One can see that for all planes P1–3 (see Figure 1) the error is kept below the allowed $6\,\mathrm{dB}$ threshold over the whole frequency range. The measurements were performed with a *RadiiSense IV* field probe having a diameter of $42\,\mathrm{mm}$, placed on a *Rohacell* foam block. To neglect field deviations caused by the sensor, a diameter which is ten times smaller than the septum height is recommended. As the septum height is $300\,\mathrm{mm}$, this requirement is slightly exceeded. Presumably, the resonances of the simulated first field requirement could not be measured because of the deviations introduced by the sensor. The second field requirement, depicted in Figure 7 and Figure 8, is also met and makes the cell compliant to *IEC 61000-4-20*. The longitudinal component increases significantly for frequencies above $500\,\mathrm{MHz}$. TEM cells usually suffer from TE_{10} mode propagation. According to [13], the approximate

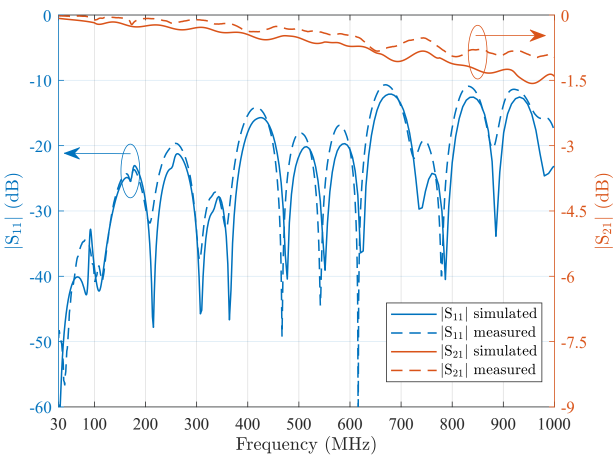

Fig. 5. Measured and simulated S-parameters.

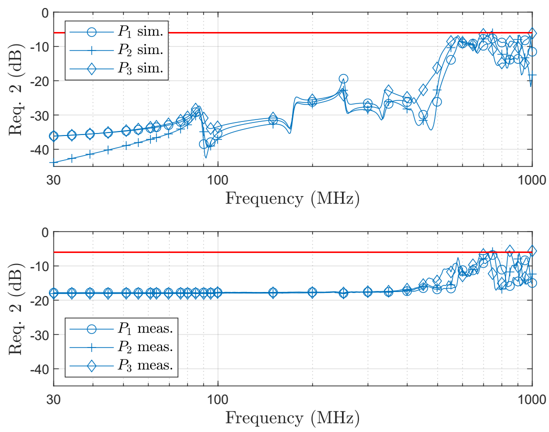

Fig. 7. Measured and simulated second field requirement: longitudinal component E_z.

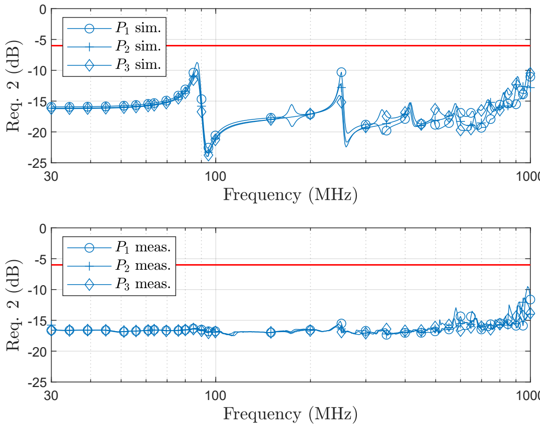

Fig. 8. Measured and simulated second field requirement: horizontal component E_x.

cutoff frequency for this mode is $f_c = c_0/(2w_c) = 500\,\mathrm{MHz}$ and correlates with the measurement results. Up to $5\,\%$ of the investigated frequencies are allowed to exceed the $-6\,\mathrm{dB}$ threshold by $4\,\mathrm{dB}$. As only $0.3\,\%$ of the simulated and $1.3\,\%$ of the measured points deviate in the allowed range, the norm is still fulfilled. Higher order modes can be suppressed by, e.g., implementing absorbers or ferrite sheets. The downside of this technique is an additional uncertainty for radiated emission testing as the desired TEM mode is influenced [14].

IV. Conclusion

The goal of this work was to increase the UTV of TEM cells using an asymmetric stripline. With the realized structure it was shown that radiated pre-compliance measurements can be made up to $1\,\mathrm{GHz}$. Compared to introduced symmetric cells, the achieved septum height of $300\,\mathrm{mm}$ is more than three times larger. By using 3D-EM simulations, the main design trade-offs regarding matching and overall length of the cell was discussed. The resulting prototype is $1.8\,\mathrm{m}$ long and the RL is kept well above the targeted $10\,\mathrm{dB}$. It was verified with an isotropic field probe that the specified UTV complies to *IEC 61000-4-20*. As the cell is laterally open, it is easy to manufacture using standard tools and having material costs below 500 €. In conclusion, a low-cost alternative for GTEM cells has been presented. The measurement results show that compliant radiated pre-compliance tests can be made in *CISPR* bands C and D for a cubic test-volume having an edge length l_{UTV} of $100\,\mathrm{mm}$.

Acknowledgement

This work was financed by *Interreg EFRE* foundation through project *AMOR ATCZ-203*.

References

[1] M. Heidemann and H. Garbe, "Using TEM waveguides according to the new IEC 61000-4-20," in *2003 IEEE International Symposium on Electromagnetic Compatibility*, vol. 1, 2003, pp. 457–460.

[2] M. Arezoomand, M. Kalantari Meybodi, and N. Noori, "Design of a TEM cell using both multi-step and piecewise linear tapering," in *2016 8th International Symposium on Telecommunications, IST 2016*, March 2017.

[3] A. Takach, F. Ndagijimana, J. Jomaah, and M. Al-Husseini, "3D-printed low-cost and lightweight TEM Cell," in *Proceedings - 2018 International Conference on High Performance Computing and Simulation, HPCS 2018*, November 2018.

[4] S. M. Satav and V. Agarwal, "Do-it-Yourself Fabrication of an Open TEM Cell for EMC Pre-compliance," *IEEE EMC Society Newsletter*, no. 20, 2008.

[5] *IEC 61000-4-20 Electromagnetic compatibility (EMC) – Part 4-20: Testing and measurement techniques – Emission and immunity testing in transverse electromagnetic (TEM) waveguides*, Std. IEC 61 000-4-20:2010.

[6] "Microwave mismatch error analysis," Hewlett-Packard, App. Note 56, 1967.

[7] *CISPR 16-1-1 Specification for radio disturbance and immunity measuring apparatus and methods - Part 1-1: Radio disturbance and immunity measuring apparatus - Measuring apparatus*, Std. CISPR 16-1-1:2019.

[8] A. Nothofer, M. Alexander, D. Bozec, A. Marvin, L. McCormack, "The use of GTEM cells for EMC measurements," National Physical Laboratory and York EMC Services Ltd., UK, Tech. Rep. 65, 2003.

[9] R. E. Collin, *Field Theory of Guided Waves*, ser. IEEE Press Series on Electromagnetic Wave Theory. Wiley, 1990.

[10] P. Robrish, "An analytic algorithm for unbalanced stripline impedance," *IEEE Transactions on Microwave Theory and Techniques*, vol. 38, no. 8, 1990.

[11] M. Koch, *Rigorous Analysis of TEM Cells*. Shaker Verlag, 1999.

[12] ANSYS. 3D EM Simulator HFSS. [Online]. Available: https://www.ansys.com/products/electronics/ansys-hfss

[13] M. T. Ma, M. Kanda, M. L. Crawford and E. B. Larsen, "A review of electromagnetic compatibility/interference measurement methodologies," *Proceedings of the IEEE*, vol. 73, no. 3, pp. 388–411, March 1985.

[14] M. L. Crawford, J. L. Workman, and C. L. Thomas, "Expanding the bandwidth of tem cells for emc measurements," *IEEE Transactions on Electromagnetic Compatibility*, vol. EMC-20, pp. 368–375, 1978.